# Effects of data quality vetoes on a search for compact binary coalescences in Advanced LIGO's first observing run

To cite this article: B P Abbott *et al* 2018 *Class. Quantum Grav.* **35** 065010

View the article online for updates and enhancements.

## Related content

- Characterization of transient noise in Advanced LIGO relevant to gravitational wave signal GW150914
B P Abbott, R Abbott, T D Abbott et al.

- The PyCBC search for gravitational waves from compact binary coalescence
Samantha A Usman, Alexander H Nitz, Ian W Harry et al.

- The characterization of Virgo data and its impact on gravitational-wave searches
J Aasi, J Abadie, B P Abbott et al.

# Effects of data quality vetoes on a search for compact binary coalescences in Advanced LIGO's first observing run

B P Abbott[1], R Abbott[1], T D Abbott[2], M R Abernathy[3],
F Acernese[4,5], K Ackley[6], C Adams[7], T Adams[8], P Addesso[9],
R X Adhikari[1], V B Adya[10], C Affeldt[10], M Agathos[11],
K Agatsuma[11], N Aggarwal[12], O D Aguiar[13], L Aiello[14,15],
A Ain[16], B Allen[10,17,18], A Allocca[19,20], P A Altin[21],
S B Anderson[1], W G Anderson[17], K Arai[1], M C Araya[1],
C C Arceneaux[22], J S Areeda[23], N Arnaud[24], K G Arun[25],
S Ascenzi[15,26], G Ashton[27], M Ast[28], S M Aston[7], P Astone[29],
P Aufmuth[18], C Aulbert[10], S Babak[30], P Bacon[31],
M K M Bader[11], P T Baker[32], F Baldaccini[33,34], G Ballardin[35],
S W Ballmer[36], J C Barayoga[1], S E Barclay[37], B C Barish[1],
D Barker[38], F Barone[4,5], B Barr[37], L Barsotti[12], M Barsuglia[31],
D Barta[39], J Bartlett[38], I Bartos[40], R Bassiri[41], A Basti[19,20],
J C Batch[38], C Baune[10], V Bavigadda[35], M Bazzan[42,43],
M Bejger[44], A S Bell[37], B K Berger[1], G Bergmann[10],
C P L Berry[45], D Bersanetti[46,47], A Bertolini[11], J Betzwieser[7],
S Bhagwat[36], R Bhandare[48], I A Bilenko[49], G Billingsley[1],
J Birch[7], R Birney[50], S Biscans[12], A Bisht[10,18], M Bitossi[35],
C Biwer[36], M A Bizouard[24], J K Blackburn[1], C D Blair[51],
D G Blair[51], R M Blair[38], S Bloemen[52], O Bock[10], M Boer[53],
G Bogaert[53], C Bogan[10], A Bohe[30], C Bond[45], F Bondu[54],
R Bonnand[8], B A Boom[11], R Bork[1], V Boschi[19,20], S Bose[55,16],
Y Bouffanais[31], A Bozzi[35], C Bradaschia[20], P R Brady[17],
V B Braginsky[49,140], M Branchesi[56,57], J E Brau[58], T Briant[59],
A Brillet[53], M Brinkmann[10], V Brisson[24], P Brockill[17],
J E Broida[60], A F Brooks[1], D A Brown[36], D D Brown[45],
N M Brown[12], S Brunett[1], C C Buchanan[2], A Buikema[12],
T Bulik[61], H J Bulten[11,62], A Buonanno[30,63], D Buskulic[8],
C Buy[31], R L Byer[41], M Cabero[10], L Cadonati[64], G Cagnoli[65,66],
C Cahillane[1], J Calderón Bustillo[64], T Callister[1], E Calloni[5,67],
J B Camp[68], K C Cannon[69], J Cao[70], C D Capano[10],

[140] Deceased, March 2016.

E Capocasa[31], F Carbognani[35], S Caride[71], J Casanueva Diaz[24], C Casentini[15,26], S Caudill[17], M Cavaglià[22], F Cavalier[24], R Cavalieri[35], G Cella[20], C B Cepeda[1], L Cerboni Baiardi[56,57], G Cerretani[19,20], E Cesarini[15,26], S J Chamberlin[72], M Chan[37], S Chao[73], P Charlton[74], E Chassande-Mottin[31], B D Cheeseboro[75], H Y Chen[76], Y Chen[77], C Cheng[73], A Chincarini[47], A Chiummo[35], H S Cho[78], M Cho[63], J H Chow[21], N Christensen[60], Q Chu[51], S Chua[59], S Chung[51], G Ciani[6], F Clara[38], J A Clark[64], F Cleva[53], E Coccia[14,26], P-F Cohadon[59], A Colla[29,79], C G Collette[80], L Cominsky[81], M Constancio[13], A Conte[29,79], L Conti[43], D Cook[38], T R Corbitt[2], N Cornish[32], A Corsi[71], S Cortese[35], C A Costa[13], M W Coughlin[60], S B Coughlin[82], J-P Coulon[53], S T Countryman[40], P Couvares[1], E E Cowan[64], D M Coward[51], M J Cowart[7], D C Coyne[1], R Coyne[71], K Craig[37], J D E Creighton[17], J Cripe[2], S G Crowder[83], A Cumming[37], L Cunningham[37], E Cuoco[35], T Dal Canton[10], S L Danilishin[37], S D'Antonio[15], K Danzmann[10,18], N S Darman[84], A Dasgupta[85], C F Da Silva Costa[6], V Dattilo[35], I Dave[48], M Davier[24], G S Davies[37], E J Daw[86], R Day[35], S De[36], D DeBra[41], G Debreczeni[39], J Degallaix[65], M De Laurentis[5,67], S Deléglise[59], W Del Pozzo[45], T Denker[10], T Dent[10], V Dergachev[1], R De Rosa[5,67], R T DeRosa[7], R DeSalvo[9], R C Devine[75], S Dhurandhar[16], M C Díaz[87], L Di Fiore[5], M Di Giovanni[88,89], T Di Girolamo[5,67], A Di Lieto[19,20], S Di Pace[29,79], I Di Palma[29,30,79], A Di Virgilio[20], V Dolique[65], F Donovan[12], K L Dooley[22], S Doravari[10], R Douglas[37], T P Downes[17], M Drago[10], R W P Drever[1], J C Driggers[38], M Ducrot[8], S E Dwyer[38], T B Edo[86], M C Edwards[60], A Effler[7], H-B Eggenstein[10], P Ehrens[1], J Eichholz[1,6], S S Eikenberry[6], W Engels[77], R C Essick[12], T Etzel[1], M Evans[12], T M Evans[7], R Everett[72], M Factourovich[40], V Fafone[15,26], H Fair[36], S Fairhurst[90], X Fan[70], Q Fang[51], S Farinon[47], B Farr[76], W M Farr[45], M Favata[91], M Fays[90], H Fehrmann[10], M M Fejer[41], E Fenyvesi[92], I Ferrante[19,20], E C Ferreira[13], F Ferrini[35], F Fidecaro[19,20], I Fiori[35], D Fiorucci[31], R P Fisher[36], R Flaminio[65,93], M Fletcher[37], J-D Fournier[53], S Frasca[29,79], F Frasconi[20], Z Frei[92], A Freise[45], R Frey[58], V Frey[24], P Fritschel[12], V V Frolov[7], P Fulda[6], M Fyffe[7], H A G Gabbard[22], J R Gair[94], L Gammaitoni[33], S G Gaonkar[16], F Garufi[5,67], G Gaur[85,95], N Gehrels[68], G Gemme[47], P Geng[87], E Genin[35], A Gennai[20], J George[48], L Gergely[96], V Germain[8], Abhirup Ghosh[97], Archisman Ghosh[97], S Ghosh[11,52], J A Giaime[2,7], K D Giardina[7], A Giazotto[20], K Gill[98], A Glaefke[37], E Goetz[38], R Goetz[6], L Gondan[92], G González[2],

J M Gonzalez Castro[19,20], A Gopakumar[99], N A Gordon[37],
M L Gorodetsky[49], S E Gossan[1], M Gosselin[35], R Gouaty[8],
A Grado[5,100], C Graef[37], P B Graff[63], M Granata[65], A Grant[37],
S Gras[12], C Gray[38], G Greco[56,57], A C Green[45], P Groot[52],
H Grote[10], S Grunewald[30], G M Guidi[56,57], X Guo[70], A Gupta[16],
M K Gupta[85], K E Gushwa[1], E K Gustafson[1], R Gustafson[101],
J J Hacker[23], B R Hall[55], E D Hall[1], G Hammond[37], M Haney[99],
M M Hanke[10], J Hanks[38], M D Hannam[90], J Hanson[7],
T Hardwick[2], J Harms[56,57], G M Harry[3], I W Harry[30],
M J Hart[37], M T Hartman[6], C-J Haster[45], K Haughian[37],
A Heidmann[59], M C Heintze[7], H Heitmann[53], P Hello[24],
G Hemming[35], M Hendry[37], I S Heng[37], J Hennig[37], J Henry[102],
A W Heptonstall[1], M Heurs[10,18], S Hild[37], D Hoak[35],
D Hofman[65], K Holt[7], D E Holz[76], P Hopkins[90], J Hough[37],
E A Houston[37], E J Howell[51], Y M Hu[10], S Huang[73],
E A Huerta[103], D Huet[24], B Hughey[98], S Husa[104],
S H Huttner[37], T Huynh-Dinh[7], N Indik[10], D R Ingram[38],
R Inta[71], H N Isa[37], J-M Isac[59], M Isi[1], T Isogai[12], B R Iyer[97],
K Izumi[38], T Jacqmin[59], H Jang[78], K Jani[64], P Jaranowski[105],
S Jawahar[106], L Jian[51], F Jiménez-Forteza[104], W W Johnson[2],
D I Jones[27], R Jones[37], R J G Jonker[11], L Ju[51], K Haris[107],
C V Kalaghatgi[90], V Kalogera[82], S Kandhasamy[22], G Kang[78],
J B Kanner[1], S J Kapadia[10], S Karki[58], K S Karvinen[10],
M Kasprzack[2,35], E Katsavounidis[12], W Katzman[7], S Kaufer[18],
T Kaur[51], K Kawabe[38], F Kéfélian[53], M S Kehl[108], D Keitel[104],
D B Kelley[36], W Kells[1], R Kennedy[86], J S Key[87], F Y Khalili[49],
I Khan[14], S Khan[90], Z Khan[85], E A Khazanov[109],
N Kijbunchoo[38], Chi-Woong Kim[78], Chunglee Kim[78],
J Kim[110], K Kim[111], N Kim[41], W Kim[112], Y-M Kim[110],
S J Kimbrell[64], E J King[112], P J King[38], J S Kissel[38], B Klein[82],
L Kleybolte[28], S Klimenko[6], S M Koehlenbeck[10], S Koley[11],
V Kondrashov[1], A Kontos[12], M Korobko[28], W Z Korth[1],
I Kowalska[61], D B Kozak[1], V Kringel[10], B Krishnan[10],
A Królak[113,114], C Krueger[18], G Kuehn[10], P Kumar[108],
R Kumar[85], L Kuo[73], A Kutynia[113], B D Lackey[36], M Landry[38],
J Lange[102], B Lantz[41], P D Lasky[115], M Laxen[7], A Lazzarini[1],
C Lazzaro[43], P Leaci[29,79], S Leavey[37], E O Lebigot[31,70],
C H Lee[110], H K Lee[111], H M Lee[116], K Lee[37], A Lenon[36],
M Leonardi[88,89], J R Leong[10], N Leroy[24], N Letendre[8],
Y Levin[115], J B Lewis[1], T G F Li[117], A Libson[12],
T B Littenberg[118], N A Lockerbie[106], A L Lombardi[119],
L T London[90], J E Lord[36], M Lorenzini[14,15], V Loriette[120],
M Lormand[7], G Losurdo[57], J D Lough[10,18], H Lück[10,18],
A P Lundgren[10], R Lynch[12], Y Ma[51], B Machenschalk[10],
M MacInnis[12], D M Macleod[2], F Magaña-Sandoval[36],

L Magaña Zertuche[36], R M Magee[55], E Majorana[29],
I Maksimovic[120], V Malvezzi[15,26], N Man[53], V Mandic[83],
V Mangano[37], G L Mansell[21], M Manske[17], M Mantovani[35],
F Marchesoni[34,121], F Marion[8], S Márka[40], Z Márka[40],
A S Markosyan[41], E Maros[1], F Martelli[56,57], L Martellini[53],
I W Martin[37], D V Martynov[12], J N Marx[1], K Mason[12],
A Masserot[8], T J Massinger[36], M Masso-Reid[37],
S Mastrogiovanni[29,79], F Matichard[12], L Matone[40],
N Mavalvala[12], N Mazumder[55], R McCarthy[38],
D E McClelland[21], S McCormick[7], S C McGuire[122],
G McIntyre[1], J McIver[1], D J McManus[21], T McRae[21],
S T McWilliams[75], D Meacher[72], G D Meadors[10,30],
J Meidam[11], A Melatos[84], G Mendell[38], R A Mercer[17],
E L Merilh[38], M Merzougui[53], S Meshkov[1], C Messenger[37],
C Messick[72], R Metzdorff[59], P M Meyers[83], F Mezzani[29,79],
H Miao[45], C Michel[65], H Middleton[45], E E Mikhailov[123],
L Milano[5,67], A L Miller[6,29,79], A Miller[82], B B Miller[82], J Miller[12],
M Millhouse[32], Y Minenkov[15], J Ming[30], S Mirshekari[124],
C Mishra[97], S Mitra[16], V P Mitrofanov[49], G Mitselmakher[6],
R Mittleman[12], A Moggi[20], M Mohan[35], S R P Mohapatra[12],
M Montani[56,57], B C Moore[91], C J Moore[125], D Moraru[38],
G Moreno[38], S R Morriss[87], K Mossavi[10], B Mours[8],
C M Mow-Lowry[45], G Mueller[6], A W Muir[90],
Arunava Mukherjee[97], D Mukherjee[17], S Mukherjee[87],
N Mukund[16], A Mullavey[7], J Munch[112], D J Murphy[40],
P G Murray[37], A Mytidis[6], I Nardecchia[15,26], L Naticchioni[29,79],
R K Nayak[126], K Nedkova[119], G Nelemans[11,52], T J N Nelson[7],
M Neri[46,47], A Neunzert[101], G Newton[37], T T Nguyen[21],
A B Nielsen[10], S Nissanke[11,52], A Nitz[10], F Nocera[35],
D Nolting[7], M E N Normandin[87], L K Nuttall[36], J Oberling[38],
E Ochsner[17], J O'Dell[127], E Oelker[12], G H Ogin[128], J J Oh[129],
S H Oh[129], F Ohme[90], M Oliver[104], P Oppermann[10],
Richard J Oram[7], B O'Reilly[7], R O'Shaughnessy[102],
D J Ottaway[112], H Overmier[7], B J Owen[71], A Pai[107], S A Pai[48],
J R Palamos[58], O Palashov[109], C Palomba[29], A Pal-Singh[28],
H Pan[73], C Pankow[82], F Pannarale[90], B C Pant[48],
F Paoletti[20,35], A Paoli[35], M A Papa[10,17,30], H R Paris[41],
W Parker[7], D Pascucci[37], A Pasqualetti[35], R Passaquieti[19,20],
D Passuello[20], B Patricelli[19,20], Z Patrick[41], B L Pearlstone[37],
M Pedraza[1], R Pedurand[65,130], L Pekowsky[36], A Pele[7],
S Penn[131], A Perreca[1], L M Perri[82], M Phelps[37],
O J Piccinni[29,79], M Pichot[53], F Piergiovanni[56,57], V Pierro[9],
G Pillant[35], L Pinard[65], I M Pinto[9], M Pitkin[37], M Poe[17],
R Poggiani[19,20], P Popolizio[35], A Post[10], J Powell[37],
J Prasad[16], J Pratt[98], V Predoi[90], T Prestegard[83], L R Price[1],

M Prijatelj[10,35], M Principe[9], S Privitera[30], R Prix[10],
G A Prodi[88,89], L Prokhorov[49], O Puncken[10], M Punturo[34],
P Puppo[29], M Pürrer[30], H Qi[17], J Qin[51], S Qiu[115],
V Quetschke[87], E A Quintero[1], R Quitzow-James[58],
F J Raab[38], D S Rabeling[21], H Radkins[38], P Raffai[92], S Raja[48],
C Rajan[48], M Rakhmanov[87], P Rapagnani[29,79], V Raymond[30],
M Razzano[19,20], V Re[26], J Read[23], C M Reed[38], T Regimbau[53],
L Rei[47], S Reid[50], D H Reitze[1,6], H Rew[123], S D Reyes[36],
F Ricci[29,79], K Riles[101], M Rizzo[102], N A Robertson[1,37],
R Robie[37], F Robinet[24], A Rocchi[15], L Rolland[8], J G Rollins[1],
V J Roma[58], J D Romano[87], R Romano[4,5], G Romanov[123],
J H Romie[7], D Rosińska[44,132], S Rowan[37], A Rüdiger[10],
P Ruggi[35], K Ryan[38], S Sachdev[1], T Sadecki[38], L Sadeghian[17],
M Sakellariadou[133], L Salconi[35], M Saleem[107], F Salemi[10],
A Samajdar[126], L Sammut[115], E J Sanchez[1], V Sandberg[38],
B Sandeen[82], J R Sanders[36], B Sassolas[65],
B S Sathyaprakash[90], P R Saulson[36], O E S Sauter[101],
R L Savage[38], A Sawadsky[18], P Schale[58], R Schilling[10,141],
J Schmidt[10], P Schmidt[1,77], R Schnabel[28], R M S Schofield[58],
A Schönbeck[28], E Schreiber[10], D Schuette[10,18],
B F Schutz[30,90], J Scott[37], S M Scott[21], D Sellers[7],
A S Sengupta[95], D Sentenac[35], V Sequino[15,26], A Sergeev[109],
Y Setyawati[11,52], D A Shaddock[21], T Shaffer[38], M S Shahriar[82],
M Shaltev[10], B Shapiro[41], P Shawhan[63], A Sheperd[17],
D H Shoemaker[12], D M Shoemaker[64], K Siellez[64],
X Siemens[17], M Sieniawska[44], D Sigg[38], A D Silva[13],
A Singer[1], L P Singer[68], A Singh[10,18,30], R Singh[2], A Singhal[14],
A M Sintes[104], B J J Slagmolen[21], J R Smith[23], N D Smith[1],
R J E Smith[1], E J Son[129], B Sorazu[37], F Sorrentino[47],
T Souradeep[16], A K Srivastava[85], A Staley[40], M Steinke[10],
J Steinlechner[37], S Steinlechner[37], D Steinmeyer[10,18],
B C Stephens[17], R Stone[87], K A Strain[37], N Straniero[65],
G Stratta[56,57], N A Strauss[60], S Strigin[49], R Sturani[124],
A L Stuver[7], T Z Summerscales[134], L Sun[84], S Sunil[85],
P J Sutton[90], B L Swinkels[35], M Szczepańczyk[98],
M Tacca[31], D Talukder[58], D B Tanner[6], M Tápai[96],
S P Tarabrin[10], A Taracchini[30], R Taylor[1], T Theeg[10],
M P Thirugnanasambandam[1], E G Thomas[45], M Thomas[7],
P Thomas[38], K A Thorne[7], E Thrane[115], S Tiwari[14,89],
V Tiwari[90], K V Tokmakov[106], K Toland[37], C Tomlinson[86],
M Tonelli[19,20], Z Tornasi[37], C V Torres[87,142], C I Torrie[1],
D Töyrä[45], F Travasso[33,34], G Traylor[7], D Trifirò[22],
M C Tringali[88,89], L Trozzo[20,135], M Tse[12], M Turconi[53],

---

[141] Deceased, May 2015.
[142] Deceased, March 2015.

D Tuyenbayev[87], D Ugolini[136], C S Unnikrishnan[99],
A L Urban[17], S A Usman[36], H Vahlbruch[18], G Vajente[1],
G Valdes[87], N van Bakel[11], M van Beuzekom[11], J F J van den
Brand[11,62], C Van Den Broeck[11], D C Vander-Hyde[36],
L van der Schaaf[11], J V van Heijningen[11], A A van Veggel[37],
M Vardaro[42,43], S Vass[1], M Vasúth[39], R Vaulin[12], A Vecchio[45],
G Vedovato[43], J Veitch[45], P J Veitch[112], K Venkateswara[137],
D Verkindt[8], F Vetrano[56,57], A Viceré[56,57], S Vinciguerra[45],
D J Vine[50], J-Y Vinet[53], S Vitale[12], T Vo[36], H Vocca[33,34],
C Vorvick[38], D V Voss[6], W D Vousden[45], S P Vyatchanin[49],
A R Wade[21], L E Wade[138], M Wade[138], M Walker[2], L Wallace[1],
S Walsh[10,30], G Wang[14,57], H Wang[45], M Wang[45], X Wang[70],
Y Wang[51], R L Ward[21], J Warner[38], M Was[8], B Weaver[38],
L-W Wei[53], M Weinert[10], A J Weinstein[1], R Weiss[12], L Wen[51],
P Weßels[10], T Westphal[10], K Wette[10], J T Whelan[102],
B F Whiting[6], R D Williams[1], A R Williamson[90], J L Willis[139],
B Willke[10,18], M H Wimmer[10,18], W Winkler[10], C C Wipf[1],
H Wittel[10,18], G Woan[37], J Woehler[10], J Worden[38], J L Wright[37],
D S Wu[10], G Wu[7], J Yablon[82], W Yam[12], H Yamamoto[1],
C C Yancey[63], H Yu[12], M Yvert[8], A Zadrożny[113],
L Zangrando[43], M Zanolin[98], J-P Zendri[43], M Zevin[82],
L Zhang[1], M Zhang[123], Y Zhang[102], C Zhao[51], M Zhou[82],
Z Zhou[82], X J Zhu[51], M E Zucker[1,12], S E Zuraw[119], J Zweizig[1]
and LIGO Scientific Collaboration and Virgo Collaboration

[1] LIGO, California Institute of Technology, Pasadena, CA 91125, United States of America
[2] Louisiana State University, Baton Rouge, LA 70803, United States of America
[3] American University, Washington, DC 20016, United States of America
[4] Università di Salerno, Fisciano, I-84084 Salerno, Italy
[5] INFN, Sezione di Napoli, Complesso Universitario di Monte S.Angelo, I-80126 Napoli, Italy
[6] University of Florida, Gainesville, FL 32611, United States of America
[7] LIGO Livingston Observatory, Livingston, LA 70754, United States of America
[8] Laboratoire d'Annecy-le-Vieux de Physique des Particules (LAPP), Université Savoie Mont Blanc, CNRS/IN2P3, F-74941 Annecy-le-Vieux, France
[9] University of Sannio at Benevento, I-82100 Benevento, Italy and INFN, Sezione di Napoli, I-80100 Napoli, Italy
[10] Albert-Einstein-Institut, Max-Planck-Institut für Gravitationsphysik, D-30167 Hannover, Germany
[11] Nikhef, Science Park, 1098 XG Amsterdam, Netherlands
[12] LIGO, Massachusetts Institute of Technology, Cambridge, MA 02139, United States of America
[13] Instituto Nacional de Pesquisas Espaciais, 12227-010 São José dos Campos, São Paulo, Brazil
[14] INFN, Gran Sasso Science Institute, I-67100 L'Aquila, Italy
[15] INFN, Sezione di Roma Tor Vergata, I-00133 Roma, Italy
[16] Inter-University Centre for Astronomy and Astrophysics, Pune 411007, India

[17] University of Wisconsin-Milwaukee, Milwaukee, WI 53201, United States of America

[18] Leibniz Universität Hannover, D-30167 Hannover, Germany

[19] Università di Pisa, I-56127 Pisa, Italy

[20] INFN, Sezione di Pisa, I-56127 Pisa, Italy

[21] Australian National University, Canberra, Australian Capital Territory 0200, Australia

[22] The University of Mississippi, University, MS 38677, United States of America

[23] California State University Fullerton, Fullerton, CA 92831, United States of America

[24] LAL, Univ. Paris-Sud, CNRS/IN2P3, Université Paris-Saclay, Orsay, France

[25] Chennai Mathematical Institute, Chennai 603103, India

[26] Università di Roma Tor Vergata, I-00133 Roma, Italy

[27] University of Southampton, Southampton SO17 1BJ, United Kingdom

[28] Universität Hamburg, D-22761 Hamburg, Germany

[29] INFN, Sezione di Roma, I-00185 Roma, Italy

[30] Albert-Einstein-Institut, Max-Planck-Institut für Gravitationsphysik, D-14476 Potsdam-Golm, Germany

[31] APC, AstroParticule et Cosmologie, Université Paris Diderot, CNRS/IN2P3, CEA/Irfu, Observatoire de Paris, Sorbonne Paris Cité, F-75205 Paris Cedex 13, France

[32] Montana State University, Bozeman, MT 59717, United States of America

[33] Università di Perugia, I-06123 Perugia, Italy

[34] INFN, Sezione di Perugia, I-06123 Perugia, Italy

[35] European Gravitational Observatory (EGO), I-56021 Cascina, Pisa, Italy

[36] Syracuse University, Syracuse, NY 13244, United States of America

[37] SUPA, University of Glasgow, Glasgow G12 8QQ, United Kingdom

[38] LIGO Hanford Observatory, Richland, WA 99352, United States of America

[39] Wigner RCP, RMKI, H-1121 Budapest, Konkoly Thege Miklós út 29-33, Hungary

[40] Columbia University, New York, NY 10027, United States of America

[41] Stanford University, Stanford, CA 94305, United States of America

[42] Dipartimento di Fisica e Astronomia, Università di Padova, I-35131 Padova, Italy

[43] INFN, Sezione di Padova, I-35131 Padova, Italy

[44] CAMK-PAN, 00-716 Warsaw, Poland

[45] University of Birmingham, Birmingham B15 2TT, United Kingdom

[46] Università degli Studi di Genova, I-16146 Genova, Italy

[47] INFN, Sezione di Genova, I-16146 Genova, Italy

[48] RRCAT, Indore MP 452013, India

[49] Faculty of Physics, Lomonosov Moscow State University, Moscow 119991, Russia

[50] SUPA, University of the West of Scotland, Paisley PA1 2BE, United Kingdom

[51] University of Western Australia, Crawley, Western Australia 6009, Australia

[52] Department of Astrophysics/IMAPP, Radboud University Nijmegen, PO Box 9010, 6500 GL Nijmegen, Netherlands

[53] Artemis, Université Côte d'Azur, CNRS, Observatoire Côte d'Azur, CS 34229, Nice cedex 4, France

[54] Institut de Physique de Rennes, CNRS, Université de Rennes 1, F-35042 Rennes, France

[55] Washington State University, Pullman, WA 99164, United States of America

[56] Università degli Studi di Urbino 'Carlo Bo', I-61029 Urbino, Italy

[57] INFN, Sezione di Firenze, I-50019 Sesto Fiorentino, Firenze, Italy

[58] University of Oregon, Eugene, OR 97403, United States of America

[59] Laboratoire Kastler Brossel, UPMC-Sorbonne Universités, CNRS, ENS-PSL Research University, Collège de France, F-75005 Paris, France

[60] Carleton College, Northfield, MN 55057, United States of America

[61] Astronomical Observatory Warsaw University, 00-478 Warsaw, Poland
[62] VU University Amsterdam, 1081 HV Amsterdam, Netherlands
[63] University of Maryland, College Park, MD 20742, United States of America
[64] Center for Relativistic Astrophysics and School of Physics, Georgia Institute of Technology, Atlanta, GA 30332, United States of America
[65] Laboratoire des Matériaux Avancés (LMA), CNRS/IN2P3, F-69622 Villeurbanne, France
[66] Université Claude Bernard Lyon 1, F-69622 Villeurbanne, France
[67] Università di Napoli 'Federico II', Complesso Universitario di Monte S.Angelo, I-80126 Napoli, Italy
[68] NASA/Goddard Space Flight Center, Greenbelt, MD 20771, United States of America
[69] RESCEU, University of Tokyo, Tokyo, 113-0033, Japan
[70] Tsinghua University, Beijing 100084, People's Republic of China
[71] Texas Tech University, Lubbock, TX 79409, United States of America
[72] The Pennsylvania State University, University Park, PA 16802, United States of America
[73] National Tsing Hua University, Hsinchu City, 30013 Taiwan, People's Republic of China
[74] Charles Sturt University, Wagga Wagga, New South Wales 2678, Australia
[75] West Virginia University, Morgantown, WV 26506, United States of America
[76] University of Chicago, Chicago, IL 60637, United States of America
[77] Caltech CaRT, Pasadena, CA 91125, United States of America
[78] Korea Institute of Science and Technology Information, Daejeon 305-806, Republic of Korea
[79] Università di Roma 'La Sapienza', I-00185 Roma, Italy
[80] University of Brussels, Brussels 1050, Belgium
[81] Sonoma State University, Rohnert Park, CA 94928, United States of America
[82] Center for Interdisciplinary Exploration & Research in Astrophysics (CIERA), Northwestern University, Evanston, IL 60208, United States of America
[83] University of Minnesota, Minneapolis, MN 55455, United States of America
[84] The University of Melbourne, Parkville, Victoria 3010, Australia
[85] Institute for Plasma Research, Bhat, Gandhinagar 382428, India
[86] The University of Sheffield, Sheffield S10 2TN, United Kingdom
[87] The University of Texas Rio Grande Valley, Brownsville, TX 78520, United States of America
[88] Dipartimento di Fisica, Università di Trento, I-38123 Povo, Trento, Italy
[89] INFN, Trento Institute for Fundamental Physics and Applications, I-38123 Povo, Trento, Italy
[90] Cardiff University, Cardiff CF24 3AA, United Kingdom
[91] Montclair State University, Montclair, NJ 07043, United States of America
[92] MTA Eötvös University, 'Lendulet' Astrophysics Research Group, Budapest 1117, Hungary
[93] National Astronomical Observatory of Japan, 2-21-1 Osawa, Mitaka, Tokyo 181-8588, Japan
[94] School of Mathematics, University of Edinburgh, Edinburgh EH9 3FD, United Kingdom
[95] Indian Institute of Technology, Gandhinagar Ahmedabad Gujarat 382424, India
[96] University of Szeged, Dóm tér 9, Szeged 6720, Hungary
[97] International Centre for Theoretical Sciences, Tata Institute of Fundamental Research, Bangalore 560012, India
[98] Embry-Riddle Aeronautical University, Prescott, AZ 86301, United States of America
[99] Tata Institute of Fundamental Research, Mumbai 400005, India
[100] INAF, Osservatorio Astronomico di Capodimonte, I-80131, Napoli, Italy

[101] University of Michigan, Ann Arbor, MI 48109, United States of America
[102] Rochester Institute of Technology, Rochester, NY 14623, United States of America
[103] NCSA, University of Illinois at Urbana-Champaign, Urbana, IL 61801, United States of America
[104] Universitat de les Illes Balears, IAC3—IEEC, E-07122 Palma de Mallorca, Spain
[105] University of Białystok, 15-424 Białystok, Poland
[106] SUPA, University of Strathclyde, Glasgow G1 1XQ, United Kingdom
[107] IISER-TVM, CET Campus, Trivandrum Kerala 695016, India
[108] Canadian Institute for Theoretical Astrophysics, University of Toronto, Toronto, Ontario M5S 3H8, Canada
[109] Institute of Applied Physics, Nizhny Novgorod, 603950, Russia
[110] Pusan National University, Busan 609-735, Republic of Korea
[111] Hanyang University, Seoul 133-791, Republic of Korea
[112] University of Adelaide, Adelaide, South Australia 5005, Australia
[113] NCBJ, 05-400 Świerk-Otwock, Poland
[114] IM-PAN, 00-956 Warsaw, Poland
[115] Monash University, Victoria 3800, Australia
[116] Seoul National University, Seoul 151-742, Republic of Korea
[117] The Chinese University of Hong Kong, Shatin, NT, Hong Kong
[118] University of Alabama in Huntsville, Huntsville, AL 35899, United States of America
[119] University of Massachusetts-Amherst, Amherst, MA 01003, United States of America
[120] ESPCI, CNRS, F-75005 Paris, France
[121] Dipartimento di Fisica, Università di Camerino, I-62032 Camerino, Italy
[122] Southern University and A&M College, Baton Rouge, LA 70813, United States of America
[123] College of William and Mary, Williamsburg, VA 23187, United States of America
[124] Instituto de Fí sica Teórica, University Estadual Paulista/ICTP South American Institute for Fundamental Research, São Paulo SP 01140-070, Brazil
[125] University of Cambridge, Cambridge CB2 1TN, United Kingdom
[126] IISER-Kolkata, Mohanpur, West Bengal 741252, India
[127] Rutherford Appleton Laboratory, HSIC, Chilton, Didcot, Oxon OX11 0QX, United Kingdom
[128] Whitman College, 345 Boyer Avenue, Walla Walla, WA 99362, United States of America
[129] National Institute for Mathematical Sciences, Daejeon 305-390, Republic of Korea
[130] Université de Lyon, F-69361 Lyon, France
[131] Hobart and William Smith Colleges, Geneva, NY 14456, United States of America
[132] Janusz Gil Institute of Astronomy, University of Zielona Góra, 65-265 Zielona Góra, Poland
[133] King's College London, University of London, London WC2R 2LS, United Kingdom
[134] Andrews University, Berrien Springs, MI 49104, United States of America
[135] Università di Siena, I-53100 Siena, Italy
[136] Trinity University, San Antonio, TX 78212, United States of America
[137] University of Washington, Seattle, WA 98195, United States of America
[138] Kenyon College, Gambier, OH 43022, United States of America
[139] Abilene Christian University, Abilene, TX 79699, United States of America

### Abstract

The first observing run of Advanced LIGO spanned 4 months, from 12 September 2015 to 19 January 2016, during which gravitational waves were directly detected from two binary black hole systems, namely GW150914 and GW151226. Confident detection of gravitational waves requires an understanding of instrumental transients and artifacts that can reduce the sensitivity of a search. Studies of the quality of the detector data yield insights into the cause of instrumental artifacts and data quality vetoes specific to a search are produced to mitigate the effects of problematic data. In this paper, the systematic removal of noisy data from analysis time is shown to improve the sensitivity of searches for compact binary coalescences. The output of the PyCBC pipeline, which is a python-based code package used to search for gravitational wave signals from compact binary coalescences, is used as a metric for improvement. GW150914 was a loud enough signal that removing noisy data did not improve its significance. However, the removal of data with excess noise decreased the false alarm rate of GW151226 by more than two orders of magnitude, from 1 in 770 yr to less than 1 in 186 000 yr.

Keywords: LIGO, detector characterization, compact binary coalescences

(Some figures may appear in colour only in the online journal)

## 1. Introduction

The Advanced Laser Interferometer Gravitational-Wave Observatory (aLIGO) is comprised of two dual-recycled Michelson interferometers [1] located in Livingston, LA (L1) and Hanford, WA (H1). A gravitational wave passing through a LIGO interferometer will induce a strain on spacetime, stretching and squeezing the 4 km arms and generating an interferometric signal at the antisymmetric port of the beamsplitter.

Advanced LIGO's first observing run (O1) lasted from 12 September 2015 to 19 January 2016. A primary goal of this observing run was the detection of gravitational waves from compact binary coalescences (CBC) [2]. This goal was achieved with the detections of GW150914 and GW151226, both signals from binary black hole systems, which marked the first direct detections of gravitational waves [3, 4]. These detections were part of a broader search for CBC signals carried out by multiple search pipelines during O1 [5–10] and searches for unmodeled transients [11–14].

Searching for gravitational waves requires an understanding of instrumental features and artifacts that can adversely affect the output of a gravitational wave search pipeline. Throughout the observing run, noisy data were identified in the form of data quality (DQ) vetoes to ensure that the analysis pipelines did not analyze data known to be contaminated with excess noise [15]. These vetoes are discussed further in section 4. This study measures the effects of removing data with excess noise on the output of PyCBC [5, 9, 10], a python-based pipeline used to search for CBC signals. Section 3 contains a brief description of the PyCBC search pipeline and its internal DQ features.

Section 2 outlines the data selection and noise characterization processes. The DQ vetoes that are generated in the noise characterization process are described in section 4. The methodology of this study is discussed in section 5. This paper focuses on two specific subsets of the O1 data set. The first data set, from 12 September–20 October 2015, was used for background estimation for GW150914. This data set is discussed in section 6. The second data set, from 3 December 2015–19 January 2016, was used for background estimation for GW151226. This data set is discussed in section 7. Section 8 describes the limiting noise sources for CBC searches.

## 2. Data selection

The strain data measured at the output of the detectors are typically non-stationary and non-Gaussian and contain noise artifacts of varying durations. The longer duration non-stationary data can affect the overall sensitivity of the search, but they do not result in loud background events as they occur on a timescale of hours. The transient noise artifacts, however, occur on a timescale of seconds and can reduce the sensitivity of CBC searches by producing loud background events.

Data quality studies must be performed to search for causes of transients in the data that generate loud events in a gravitational wave search. If the source of noise is identified, a veto is generated to flag times when transient noise makes the data unsuitable for analysis. Section 4 describes DQ vetoes that are used to indicate when the detector data are known to have excess noise [15–18]. The exception to this process is gating [5], which is a feature internal to the CBC searches. This gating, which is applied independently of DQ vetoes, uses a window function to remove times containing large transients from the input data stream.

## 3. The PyCBC search pipeline

The PyCBC pipeline is designed to search for gravitational wave transients from CBCs [5]. It employs a matched filter algorithm, which correlates expected CBC waveforms with detector data and outputs a ranking statistic, the signal-to-noise ratio (SNR). If the ranking statistic exceeds a specified threshold, an event, or 'trigger', is generated. The SNR of each trigger is weighted based on a signal consistency test [19], resulting in a refined ranking statistic called re-weighted SNR. Section 3.1 discusses this signal consistency test further.

To perform this search, the matched filter algorithm needs to know what to search for. A collection of model CBC waveforms is generated before the analysis [20, 21]. Each of these waveforms is called a template and the full collection of waveforms is referred to as the template bank. This template bank is constructed to span the astrophysical parameter space included in the search [22]. Each waveform is defined by the mass and spin of each compact object in the binary system. It is often convenient to combine the effects of each object's spin into one parameter called effective spin $\chi_{\text{eff}}$, which is the mass-weighted spin of the system [7]. The mass of the binary system is often represented by the chirp mass $\mathcal{M}$ [23], which is used to parameterize gravitational wave signals in general relativity.

The search algorithm is run separately at each detector and a set of single detector triggers is generated. The two sets of single detector triggers are then compared to search for any events that were recorded within a 15 ms coincidence window, which reflects the travel time of a gravitational wave between the detectors and allows for uncertainty in the arrival time of a signal [5]. Any triggers that are found in coincidence with the same source parameters in both detectors represent potential gravitational wave signals and are referred to as foreground

events. Some of these foreground events will be chance coincidences between noise in each detector, which is expected given the number of events in each data set.

To determine the statistical significance of foreground events, a background distribution is generated using a time shift technique [5]. The statistical significance of any candidate gravitational wave is then quantified by calculating the rate of background events from detector noise that are at least as loud as the candidate event. This statistic is called the false alarm rate (FAR). Any loud triggers that appear as the result of instrumental transients will extend the background distribution and the influence the measured false alarm rate. The purpose of the DQ effort as a whole is thus two-fold: to ensure that the search is using representative detector data in the background noise estimation and to suppress the rate of loud events that will pollute both the background and the foreground distributions.

### 3.1. $\chi^2$ signal consistency test

A further layer of effective DQ that is internal to the PyCBC pipeline is the application of the $\chi^2$ signal consistency test [19]. The SNR produced by the matched filter is an integral in the frequency domain. The $\chi^2$ test divides each CBC waveform into frequency bins of equal power, checking that the SNR is distributed as a function of frequency as expected from an actual CBC signal. Each trigger that comes out of the matched filter search is down-weighted based on the results of the $\chi^2$ test. This is folded into a new ranking statistic for CBC triggers, which is called re-weighted SNR and is denoted by $\hat{\rho}$. The ranking statistic for coincident events in the PyCBC search is the network re-weighted SNR, $\hat{\rho}_c$, which is the quadrature sum of the re-weighted SNR from each detector. Since a real signal has a power distribution that matches the template waveform, it will not be down-weighted by the $\chi^2$ test; the SNR and the re-weighted SNR will be the same.

This test is extremely powerful, as shown in figure 1, which shows the distribution of single detector PyCBC triggers generated from 12 September to 20 October 2015. Figure 1(a) shows the distribution of triggers in SNR. The extensive tail of triggers with high SNR, which extends beyond SNR 100, is down-weighted in the re-weighted SNR distribution, leaving behind a tail that extends to $\hat{\rho} \approx 10.5$ as seen in figure 1(b). This re-weighted SNR tail represents the loudest single detector background triggers in the CBC search. Investigating this set of loudest background triggers guides DQ efforts in defining the current limiting noise sources to the CBC search.

## 4. Data quality vetoes

As seen in figure 1, the $\chi^2$ test is a powerful tool, but there is still a considerable tail in the single detector trigger distribution. This tail is often caused by transient instrumental noise. If these noise sources can be linked to a systematic instrumental cause or a period of highly irregular instrumental performance, they can be flagged and removed from the analysis in the form of a DQ veto.

DQ vetoes indicate times that are unsuitable for analysis or are likely to produce false alarm gravitational wave triggers. These vetoes are constructed by ~200 000 witness sensors that continuously monitor LIGO detectors and their environment [15]. Before a witness sensor is used to generate a DQ veto, its sensitivity to a genuine gravitational wave signal is assessed to ensure true signals are not unnecessarily removed from analysis. To test this, a gravitational wave signal is simulated by electromagnetically controlling the motion of the detector optics. If a witness sensor is observed to be sensitive to such an injected signal, it will be considered unsafe for generating DQ vetoes.
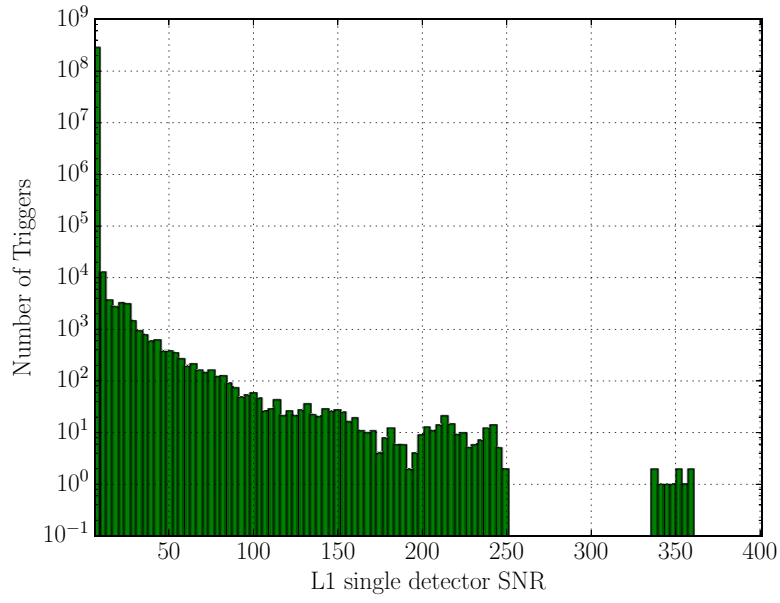
(a)
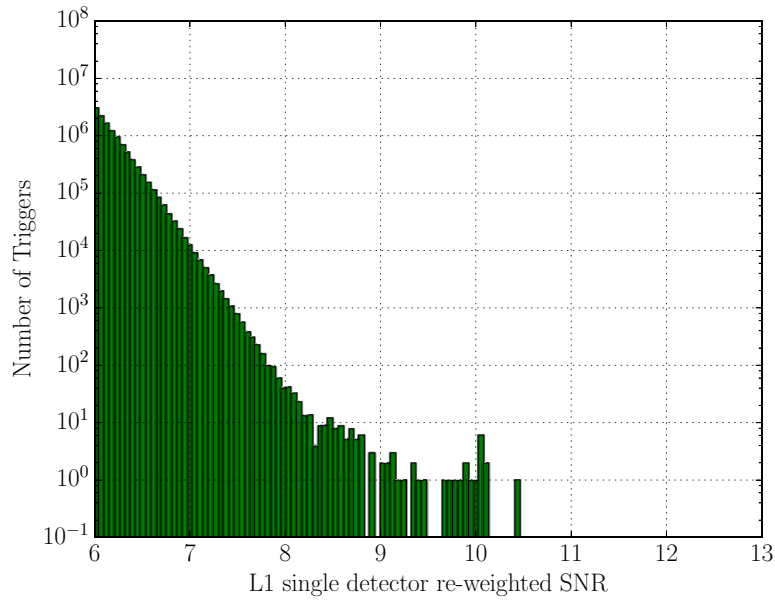


(b)

**Figure 1.** Histograms of single detector triggers from the Livingston (L1) detector. These triggers were generated using data from 12 September to 20 October 2015. These histograms contain triggers from the entire template bank, but exclude any triggers found in coincidence between the two detectors. (a) A histogram of single detector triggers in SNR. The tail of this distribution extends beyond SNR = 100. (b) A histogram of single detector triggers in re-weighted SNR. The chi-squared test down-weights the long tail of SNR triggers in the re-weighted SNR distribution. The triggers found using only the Hanford detector have a similar distribution.

As an example, a veto was generated during O1 to mark times when an electronics fault caused amplitude fluctuations in the radio frequency (RF) sidebands used to sense and control LIGO's optical cavities. These amplitude fluctuations introduced noise into the feedback loops controlling the motion of the LIGO optics. This excess motion coupled into the output of the detector and created transient, broadband noise artifacts. A witness sensor monitoring the amplitude stabilization control signal for the RF sidebands was found to be correlated to the excess noise in the detector output. A threshold was established to indicate when the amplitude fluctuations were significant enough to couple into the detector output and any times where the fluctuation amplitude exceeded this threshold were marked as unfit for astrophysical analysis. The process of generating this veto is further detailed in appendix A of [15].

Other examples of noise sources that were vetoed in O1 are photodiode saturations, analog-to-digital converter (ADC) and digital-to-analog converter (DAC) overflows, elevated seismic noise, and computer failures. These DQ vetoes were generated using a process similar to that used to veto the RF amplitude fluctuation noise.

DQ vetoes are produced for all analysis time based on systematic instrumental conditions without any regard for the presence of gravitational wave signals. All data are treated equally; the removal of data with excess noise has the ability to remove real gravitational wave signals as well as background events. The same set of DQ vetoes was applied by all CBC searches in O1 and will be released with any public data to ensure that astrophysical results are reproducible. Further details on DQ vetoes applied in the first observing run are available in a paper detailing the transient noise in the detectors at the time of GW150914 [15].

## 5. Measuring the effects of data quality vetoes

To test the effects of DQ vetoes, the PyCBC search pipeline was run with and without applying vetoes. The only vetoes that were used in all runs are those that indicate that the data were not properly calibrated, that a data dropout occurred, or that there were test signals being injected into the detectors. Gating is internal to the search pipeline and was applied in all of the analyses. Two methods were used to understand the effects of applying vetoes. The first, described in section 5.1, considers the average sensitivity of the search pipeline to gravitational wave signals. The second, described in section 5.2, compares the measured search backgrounds and the false alarm rates of recovered gravitational wave signals.

### 5.1. Measuring search sensitivity

The metric used to measure the sensitivity of the search pipeline is sensitive volume. Sensitive volume is measured by injecting simulated gravitational wave signals into the data and attempting to recover them using the search [5]. The ability of the pipeline to recover signals at a given false alarm rate is then measured by analyzing the number of missed and recovered injections.

In addition to the sensitive volume, the amount of time used in the analysis must be considered when removing noisy data. If a search is rejecting too much data, it will miss the opportunity to detect signals. To address this, the sensitive volume of the search is multiplied by the amount of analysis time to create a new metric called VT. If time is removed from an analysis, the sensitive volume of the search must increase to make up for the shorter analyzed time.

The sensitivity of a search varies as a function of the significance threshold set for candidate events. The VT ratios are therefore calculated at both the 1 per 100 yr and the 1 per 1000 yr levels. These significance levels are expressed as inverse false alarm rates (IFAR).

*5.2. Comparing search backgrounds*

In the first observing run, the bank of CBC waveform templates used in the PyCBC search was divided into three bins [22]. The significance of any candidate gravitational wave found in coincidence between the two detectors is calculated relative to the background in its bin. Waveforms with different parameters will respond to instrumental transients in different ways. This binning is performed so that any foreground triggers are compared to a background generated from similar waveforms. As such, the effects of removing data from the PyCBC search are variable depending on which bin is considered. The actual gravitational wave signals discovered in the PyCBC search, GW150914 and GW151226, were part of a full search that was broken into 3 bins but reported as a single table of results. Because of this, their reported false alarm rates include a trials factor of 3. The background distributions shown in sections 6 and 7 were measured on a bin-by-bin basis, so the cumulative trigger rates have not been divided by 3.

The first bin is called the binary neutron star (BNS) bin and contains all waveforms with $\mathcal{M} < 1.74$. The second bin is the edge bin, which is defined based on the peak frequency $f_{peak}$ of each CBC waveform. These waveforms are typically shorter in duration than binary neutron star waveforms and are comprised of both binary black hole (BBH) and neutron star-black hole (NSBH) binary waveforms. Waveforms in the edge bin typically have high masses and negative $\chi_{eff}$. In this analysis, the edge bin contained waveforms with $f_{peak} < 100$ Hz. The third bin is the bulk bin, which contains all remaining waveforms needed to span the parameter space of the search. This contains BBH and NSBH waveforms with a variety of mass ratios and spins.

## 6. Analysis containing GW150914

The analysis containing GW150914 lasted from 12 September–20 October 2015 and contained a total of 18.2 d of coincident detector data. Of this 18.2 d, 7.7% was considered unfit for astrophysical analysis and was removed from the data set.

*6.1. Search sensitivity*

To measure the effects of DQ vetoes on the sensitivity of the search, the analysis containing GW150914 was performed with and without applying data quality vetoes. The resulting measurements of VT were divided to calculate a VT ratio.

Figure 2 shows the change in VT when vetoes are applied for two values of IFAR and several chirp mass bins. The lowest chirp mass bin contains BNS signals and does not show any improvement in sensitivity when DQ vetoes are applied. This is discussed further in section 6.2. Since the bulk and edge bins contain systems with a large range of masses that can respond in different ways to instrumental artifacts, these higher mass bins have been split for sensitivity estimation. The higher mass bins in figure 2 are binned linearly in $\ln(\mathcal{M})$. The higher chirp mass bins show an improvement in search sensitivity for both values of IFAR.

*6.2. BNS bin*

Binary neutron star systems have the longest waveforms used in the search pipelines. Since these signals spend ∼10–100 s in LIGO's sensitive band, the $\chi^2$ test is effective at discriminating between binary neutron star signals and transient noise, which have a duration of ∼1 s.
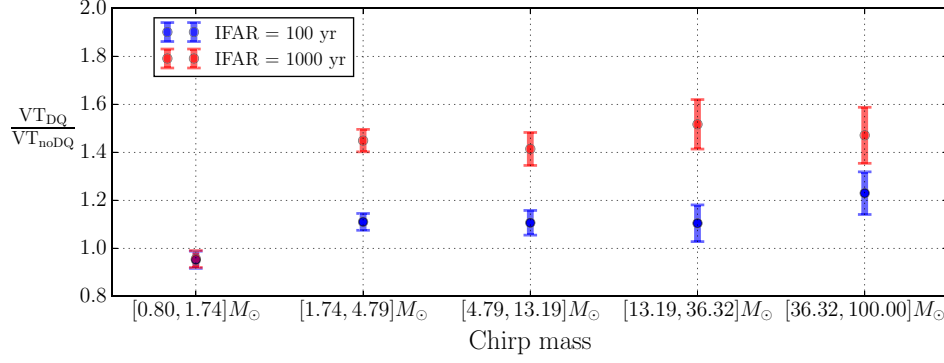
**Figure 2.** The change in search sensitivity when DQ vetoes are applied for the analysis containing GW150914. The error bars show the $1\,\sigma$ error from each VT calculation combined in quadrature. The lowest chirp mass bin, which contains BNS signals, does not show any improvement in sensitivity. For marginally significant signals at IFAR = 100, the measured value of VT increases by 3–32% in higher chirp mass bins. For highly significant signals at IFAR = 1000, the measured value of VT increases by 34–62% in higher chirp mass bins.
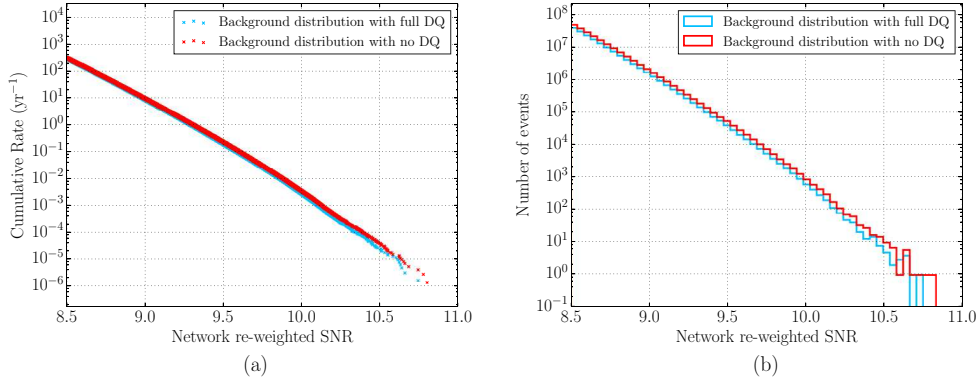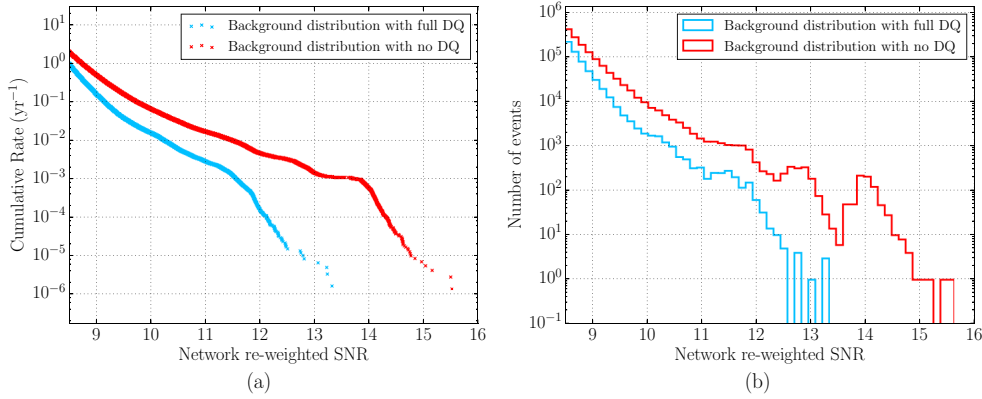


**Figure 3.** The background distribution in the BNS bin before and after applying DQ vetoes for the analysis containing GW150914. (a) The cumulative rate of background triggers in the BNS bin as a function of re-weighted SNR. (b) A histogram of background triggers in the BNS bin. The red traces indicate the distribution of background triggers without noisy data removed, the cyan traces indicate the distribution of background triggers with all DQ vetoes applied. The BNS bin shows no significant improvement in cumulative rate.

Figure 3 shows the background distribution of the BNS bin in the PyCBC search for the analysis containing GW150914. As expected, since waveforms in the BNS bin are not as susceptible to instrumental transients, the background distribution does not change significantly when noisy data are removed from the analysis.

### 6.3. Bulk bin

Figure 4 shows the background distribution in the bulk bin for the analysis containing GW150914. If noisy data are not removed from the analysis, there is a shoulder in the
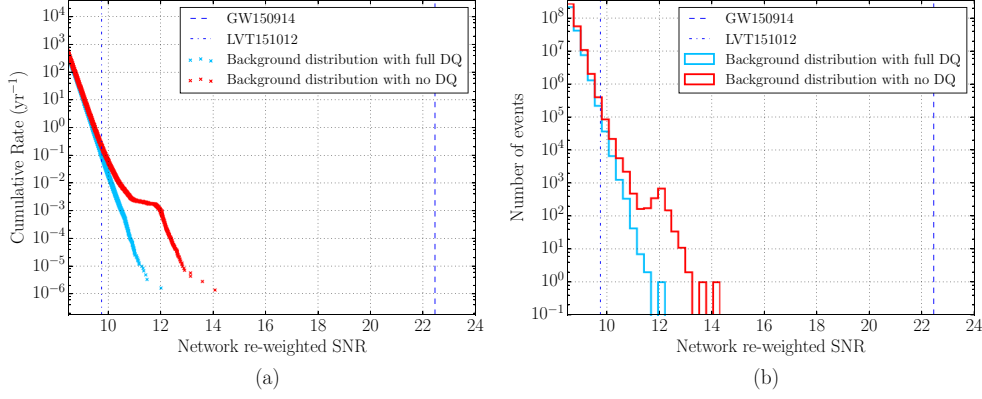
**Figure 4.** The background distribution in the bulk bin before and after applying DQ vetoes for the analysis containing GW150914. (a) The cumulative rate of background triggers in the bulk bin as a function of re-weighted SNR. (b) A histogram of background triggers in the bulk bin. The red traces indicate the distribution of background triggers without noisy data removed and the cyan traces indicate the distribution of background triggers with all DQ vetoes applied. When vetoes are not applied, there is a shoulder in the distribution that limits the sensitivity of the search. The dash-dotted line indicates the network re-weighted SNR of LVT151012. The dashed line indicates the network re-weighted SNR of GW150914, which is the loudest event in this bin for both configurations.

**Table 1.** Table of bulk bin false alarm rates for LVT151012.

| Analysis configuration | False alarm rate ($yr^{-1}$) |
| --- | --- |
| All vetoes applied | 0.33 |
| No vetoes applied | 0.69 |

distribution that extends to $\hat{\rho}_c = 14$, which limits the sensitivity of the search in the region where $11 < \hat{\rho}_c < 14$.

*6.3.1. LVT151012.*   The second most significant trigger in the analysis containing GW150914 was LVT151012, recorded on 12 October 2015 [22, 24]. This trigger was recovered in the bulk bin with $\hat{\rho}_c = 9.75$ and a false alarm rate of 0.33 $yr^{-1}$. This is not significant enough to be claimed as a confident detection. The false alarm rate decreases by a factor of 2.1 when DQ vetoes are applied, as shown in table 1.

## 6.4. Edge bin

Figure 5 shows the background distribution in the edge bin for the analysis containing GW150914. There is a visible separation between the two curves that increases for larger values of $\hat{\rho}_c$, indicating that the ability of the search pipeline to make confident detections is diminished in this region.

*6.4.1. GW150914.*   The gravitational wave signal GW150914 was detected on September 14, 2015 with $\hat{\rho}_c = 23.6$ [3]. The false alarm rate of GW150914 does not change significantly when noisy data are removed from the analysis, which can be seen in table 2. This is an expected result as GW150914 is louder than the entire background distribution in the bulk bin.

17

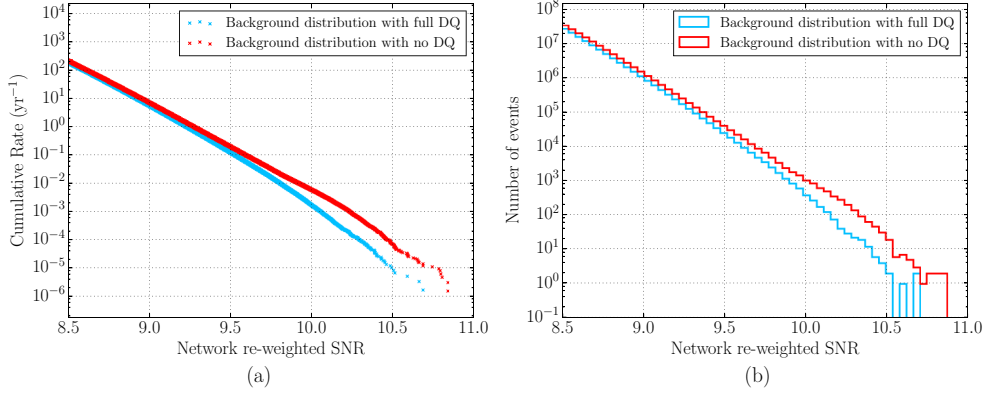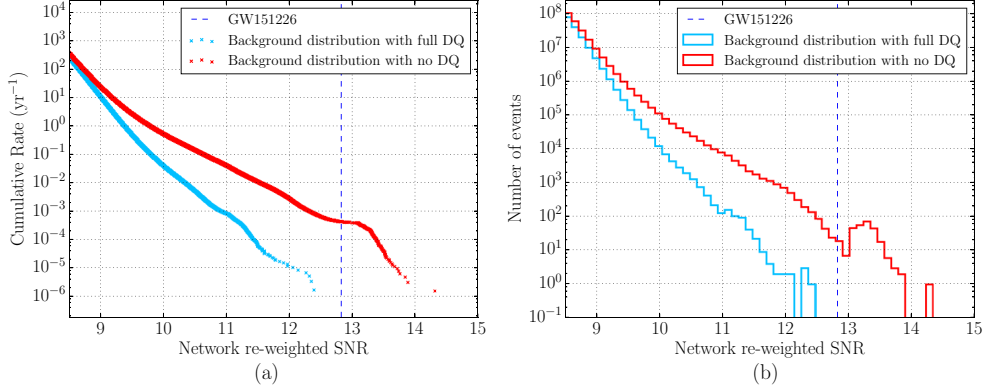(a)                                                    (b)

**Figure 5.** The background distribution in the edge bin before and after applying DQ vetoes for the analysis containing GW150914. (a) The cumulative rate of background triggers in the edge bin as a function of re-weighted SNR. (b) A histogram of background triggers in the edge bin. The red traces indicate the distribution of background triggers without noisy data removed from the analysis and the cyan traces indicate the distribution of background triggers with all data quality vetoes applied.

**Table 2.** Table of bulk bin false alarm rates for GW150914. GW150914 is loud enough that its false alarm rate does not change significantly when noisy data are removed from the analysis. Any change in false alarm rate is due to small changes in the total analysis time after data removal.

| Analysis configuration | False alarm rate ($yr^{-1}$) |
| --- | --- |
| All vetoes applied | $<5.17 \times 10^{-6}$ |
| No vetoes applied | $<4.43 \times 10^{-6}$ |

## 7. Analysis containing GW151226

The extended analysis containing GW151226 lasted from 3 December 2015–19 January 2016 and contained a total of 16.7 days of coincident detector data. Of this 16.7 days, 6.5% was considered unfit for astrophysical analysis and was removed from the data set.

### 7.1. Search sensitivity

Figure 6 shows the change in VT when DQ vetoes are applied to the analysis containing GW151226. For this analysis, the lowest chirp mass bin, which contains BNS signals, shows a slight improvement when vetoes are applied. This improvement is discussed further in section 7.2. Similar to the analysis containing GW150914, the higher chirp mass bins show an improvement in search sensitivity for both values of IFAR.

### 7.2. BNS bin

As expected from figure 6, there is a small improvement in the BNS background distribution when DQ vetoes are applied. Figure 7 shows the background distributions in the BNS bin with and without noisy data removed. Although the $\hat{\rho}_c$ of the loudest background event does not change considerably, there is a noticeable gap between the two background
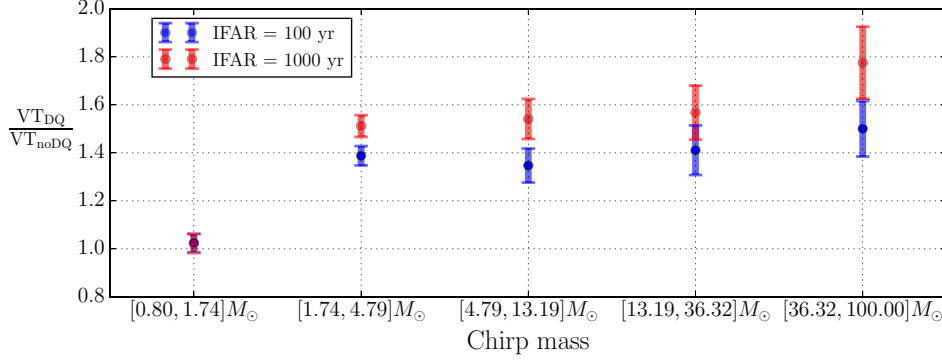
**Figure 6.** The change in search sensitivity when DQ vetoes are applied for the analysis containing GW151226. The error bars show the $1\sigma$ error from each VT calculation combined in quadrature. The lowest chirp mass bin, which contains BNS signals, shows a small improvement in sensitivity when vetoes are applied, though the error bars are consistent with a VT ratio of 1. For marginally significant signals at IFAR = 100, the measured value of VT increases by 27–62% in higher chirp mass bins. For highly significant signals at IFAR = 1000, the measured value of VT increases by 45–90% in higher chirp mass bins.
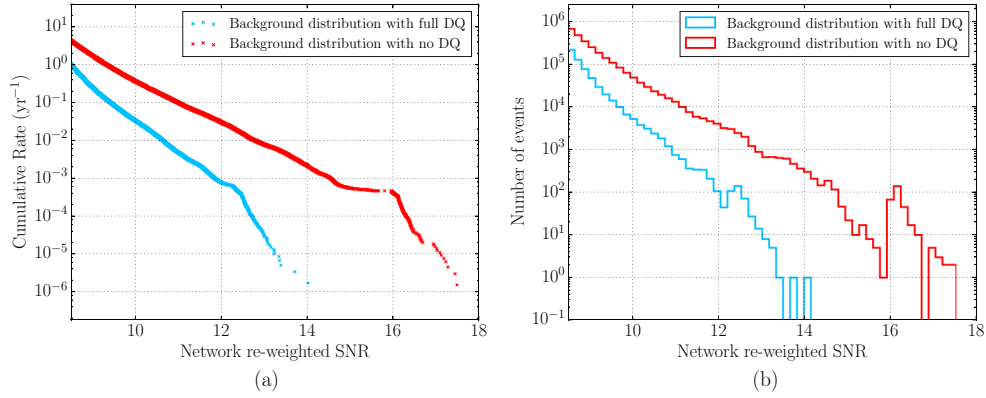


**Figure 7.** The background distribution in the BNS bin before and after applying DQ vetoes for the analysis containing GW151226. (a) The cumulative rate of background triggers in the BNS bin as a function of re-weighted SNR. (b) A histogram of background triggers in the BNS bin. The red traces indicate the distribution of background triggers without noisy data removed and the cyan traces indicate the distribution of background triggers with all vetoes applied.

distributions that is visible at $\hat{\rho}_c > 9.7$ and widens to an order of magnitude difference in FAR at $\hat{\rho}_c \approx 10.5$.

## 7.3. Bulk bin

The background distribution in the bulk bin changes significantly when DQ vetoes are applied, which is shown in figure 8. There is a visible difference between the two distributions beginning at $\hat{\rho}_c = 9$. The difference in cumulative rate reaches an order of magnitude at $\hat{\rho}_c \sim 10$

**Figure 8.** The background distribution in the bulk bin before and after applying DQ vetoes for the analysis containing GW151226. (a) The cumulative rate of background triggers in the bulk bin as a function of re-weighted SNR. (b) A histogram of background triggers in the bulk bin. The red traces indicate the distribution of background triggers with no data removed from the analysis. The cyan traces indicate the distribution of background triggers with all DQ vetoes applied. The dotted line indicates GW151226, which was recovered with $\hat{\rho}_c = 12.7$. If DQ vetoes are not applied, GW151226 is no longer louder than the entire background distribution.

**Table 3.** Table of bulk bin false alarm rates of GW151226. The false alarm rate of GW151226 increases from less than 1 in 186 000 yr to 1 in 770 yr if data with excess noise is not removed from the analysis.

| Analysis configuration | False alarm rate ($\text{yr}^{-1}$) |
|---|---|
| All vetoes applied | $<5.39 \times 10^{-6}$ |
| No vetoes applied | $1.30 \times 10^{-3}$ |

and continues to grow for larger values of $\hat{\rho}_c$. The reduction of the background distribution through the application of DQ vetoes is particularly impactful for GW151226, which is discussed in section 7.3.1.

*7.3.1. GW151226.*   The second binary black hole system discovered in the first observing run, GW151226 [4], is indicated by the vertical dotted line at $\hat{\rho}_c = 12.7$ in figure 8. When noisy data are removed from the analysis, the background distribution in the bulk bin is reduced and GW151226 is the loudest event in the analysis. The false alarm rate of GW151226 decreases by over two orders of magnitude, resulting in a clear detection. The false alarm rates before and after DQ vetoes are applied are listed in table 3.

### 7.4. Edge bin

Figure 9 shows the background distribution in the edge bin before and after DQ vetoes have been applied. The background distribution of the edge bin in the analysis containing GW151226 is significantly reduced for all values of $\hat{\rho}_c$ when DQ vetoes are applied.

(a)                                                                (b)

**Figure 9.** The background distribution in the edge bin before and after applying DQ vetoes for the analysis containing GW151226. (a) The cumulative rate of background triggers in the edge bin as a function of re-weighted SNR. (b) A histogram of background triggers in the bulk bin. The red traces indicate the distribution of background triggers without removing noisy data and the cyan traces indicate the distribution of background triggers with all vetoes applied.
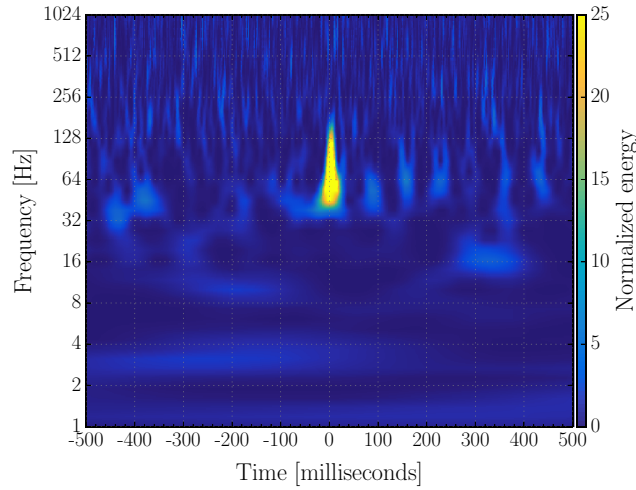


**Figure 10.** A time-frequency representation [25] of the Livingston strain channel at the time of a blip transient. This visualization of a blip transient demonstrates their typical features: band-limited, short duration, and little visible frequency structure.

## 8. Limiting noise sources

The sensitivity of the search is limited by instrumental features that result in high $\hat{\rho}_c$ triggers and tails in the background distributions. This section uses two particular instrumental noise sources from the analysis containing GW150914 as case studies. These are examples of noise sources that are not able to be vetoed using existing algorithms as they are not captured by any existing witness sensors in the detectors.
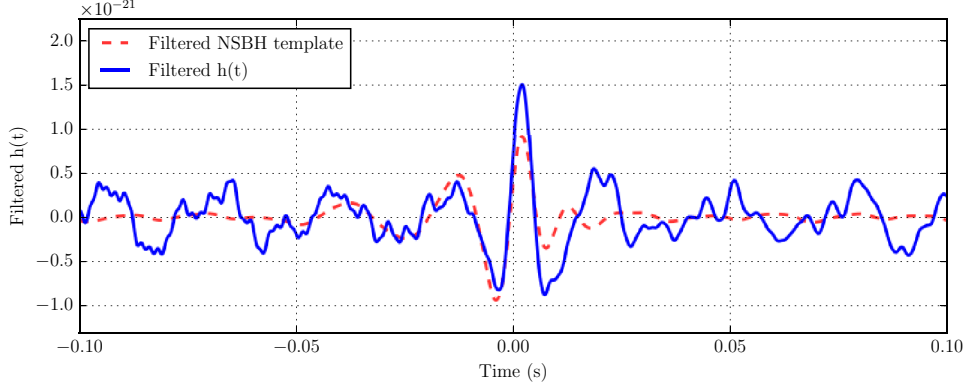
**Figure 11.** A filtered time-domain representation of the Livingston strain channel $h(t)$ at the time of a blip transient. The dotted line is a filtered CBC waveform that reported a high re-weighted SNR value at the time of the blip transient. Both sets of data have been zero-phase bandpass filtered to isolate the frequency range that aLIGO is sensitive to. The short duration and high overlap of these two curves causes the $\chi^2$ to be ineffective at down-weighting these transients.
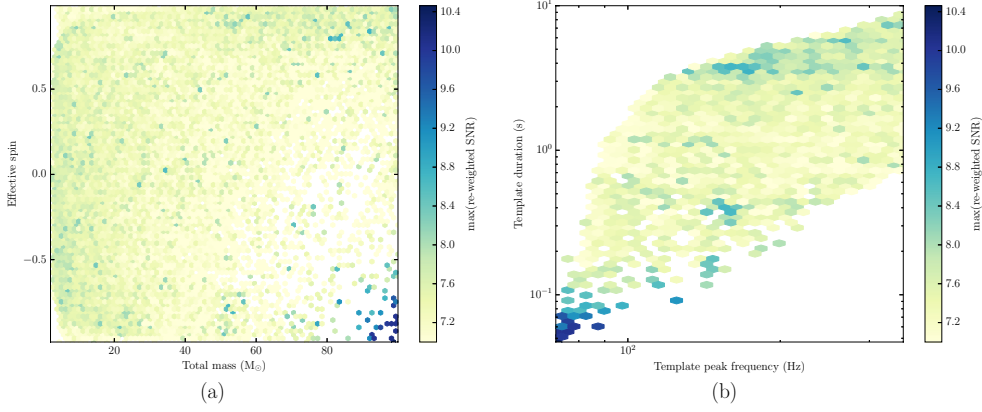


**Figure 12.** Single detector triggers from the Livingston detector during the analysis containing GW150914. (a) Triggers binned by total mass and effective spin. The highest re-weighted SNR triggers are constrained to the bottom corner of the plot, bounded by $M_{\text{total}} > 80$ and $\chi_{\text{eff}} < -0.5$. (b) Triggers binned by the peak frequency and duration of the template waveform. The loudest triggers in re-weighted SNR are constrained to the area of the parameter space with template durations $<0.1$ s. The small cluster of loud triggers with a template duration of roughly 4 s corresponds to the 60–200 Hz noise discussed in section 8.2.

## 8.1. Blip transients

Blip transients [15] are band-limited noise transients that occur in both the Hanford and Livingston detectors. They do not occur in coincidence between the two LIGO detectors and are not candidate gravitational wave signals. Due to their short duration in LIGO's sensitive frequency band, the $\chi^2$ test is not as effective at down-weighting these noise transients and they have been a common source of high re-weighted SNR background triggers. Figure 10 shows a time-frequency representation of a blip transient.
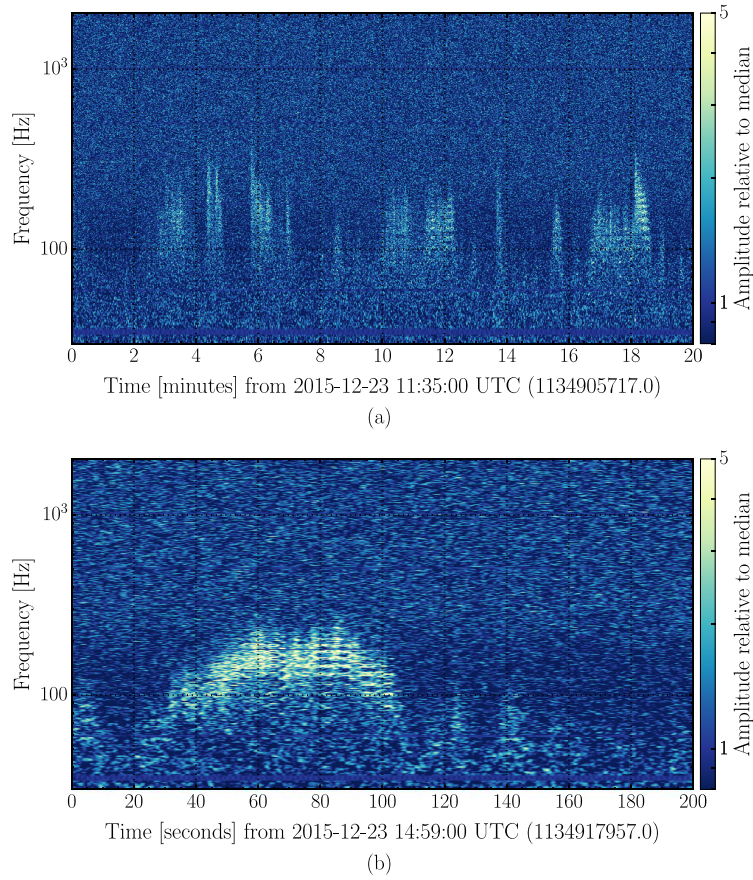
**Figure 13.** Time-frequency spectrograms of the 60–200 Hz noise. (a) A 20 min time scale shows the 60–200 Hz noise appearing for several minutes at a time. This time scale and frequency range is damaging to CBC searches and has often been found responsible for loud background events. (b) A 200 s time scale reveals the arc-like shape of the noise in the time-frequency plane. This period of noise caused a loud trigger in the PyCBC background.

Figure 11 shows a time-domain representation of a blip transient in the Livingston strain channel. The dotted line on top of the strain data represents a template waveform that reported a high re-weighted SNR at the time of this blip transient. Both curves have been filtered to isolate the parts of the signal that are in LIGO's sensitive frequency band. The template waveform is a high mass system ($M_{\text{total}} = 98.34$ M$_\odot$) with an anti-aligned effective spin of $-0.97$. This waveform is among the shortest duration templates used in the analysis, spending less than 0.1 s in LIGO's sensitive frequency band.

The region of the astrophysical parameter space where the $\chi^2$ test is ineffective at down-weighting blip transients is small. This is demonstrated in figure 12, which shows triggers from the Livingston detector during the analysis containing GW150914. Each point represents the highest single detector re-weighted SNR measured in that region of the parameter space. Figure 12(a) shows this trigger set binned by total mass and effective spin. Templates that overlap with blip transients and produce high re-weighted SNR triggers, such as the template plotted in figure 11, are constrained to the region where $M_{\text{total}} > 80$M$_\odot$ and $\chi_{\text{eff}} < -0.5$. This

region contains only 65 waveform templates out of 249077 total waveforms in the template bank; the majority of the template bank is capable of rejecting blip glitches using the $\chi^2$ test. Blip glitches that cause loud background events in this region of the template bank populate the tail of the background distribution in the edge bin and limit search sensitivity in that bin.

The region of the template bank where the $\chi^2$ test is ineffective can also be visualized in terms of the duration of the template waveform. Figure 12(b) shows the same trigger set binned by the peak frequency and duration of the template waveform. In this view of the parameter space, the templates with the highest re-weighted SNR are contrained to the region where the duration of the template in LIGO's sensitive frequency band is less than 0.1 s. In this region, the duration of the template is on the same time scale as instrumental transients such as blip transients.

Mitigation of blip transients is a high priority but is difficult since they do not couple into instrumental witness sensors and are not high enough in amplitude to be removed by the gating process. Since an instrumental cause has not yet been identified, a modified ranking statistic [26] that is capable of better discriminating blip transients from gravitational wave signals has been developed and implemented for the second observing run.

### 8.2. 60–200 Hz noise

A second problematic noise source that was present at Livingston during the first observing run was the '60–200 Hz' noise. Figure 13 shows a time-frequency visualization of this noise on both 200 s and 20 min time scales. This noise source appears for several minutes at a time as arc-like patterns in the time-frequency plane. This noise source causes loud background triggers when analyzing the Livingston data, including the band of triggers with a template duration of $\sim$4 s in figure 12(b). Although the arc-like patterns in figure 13(b) are similar to those caused by scattered light [27], the exact cause of this noise is not yet fully understood.

## 9. Conclusions

Data quality vetoes improved the sensitivity of the PyCBC search in Advanced LIGO's first observing run. Although the sensitivity of the search to BNS signals was not dramatically affected, VT improved significantly for higher mass sources when DQ vetoes are applied.

The gravitational wave signal GW150914 was strong enough that it was louder than all background events regardless of what data were removed from the search. As such, DQ vetoes did not improve its significance. The false alarm rate of LVT151012, which occurred during the same analysis period, was improved from 0.69 yr$^{-1}$ to 0.33 yr$^{-1}$ when vetoes were applied. The false alarm rate of the second gravitational wave signal discovered in O1, GW151226, was decreased by over two orders of magnitude when DQ vetoes were applied, which resulted in a clear detection. The production and application of DQ vetoes was critical for increasing overall sensitivity in Advanced LIGO's first observing run and similar methods were employed during the second observing run.

## Acknowledgments

## References

[1]  Aasi J *et al* 2015 Advanced LIGO *Class. Quantum Grav.* **32** 074001
[2]  Babak S *et al* 2013 Searching for gravitational waves from binary coalescence *Phys. Rev.* D **87** 024033
[3]  Abbott B P *et al* 2016 Observation of gravitational waves from a binary black hole merger *Phys. Rev. Lett.* **116** 061102
[4]  Abbott B *et al* 2016 GW151226: observation of gravitational waves from a 22-solar-mass binary black hole coalescence *Phys. Rev. Lett.* **116** 241103
[5]  Usman S *et al* 2016 An improved pipeline to search for gravitational waves from compact binary coalescence *Class. Quantum Grav.* **33** 215004
[6]  Cannon K *et al* 2012 Toward early-warning detection of gravitational waves from compact binary coalescence *Astrophys. J.* **748** 136
[7]  Privitera S *et al* 2014 Improving the sensitivity of a search for coalescing binary black holes with nonprecessing spins in gravitational wave data *Phys. Rev.* D **89** 024003
[8]  Messick C *et al* 2017 Low-latency analysis framework for the prompt discovery of compact binary mergers in gravitational wave data *Phys. Rev.* D **95** 042001
[9]  Nitz A *et al* 2017 Ligo-cbc/pycbc: O2 production release 11 https://doi.org/10.5281/zenodo.556097
[10]  Dal Canton T *et al* 2014 Implementing a search for aligned-spin neutron star-black hole systems with advanced ground based gravitational wave detectors *Phys. Rev.* D **90** 082004

[11] Abbott B P *et al* 2016 Observing gravitational-wave transient GW150914 with minimal assumptions *Phys. Rev.* D **93** 122004
[12] Klimenko S *et al* 2008 Coherent method for detection of gravitational wave bursts *Class. Quantum Grav.* **25** 114029
[13] Lynch R *et al* 2017 An information-theoretic approach to the gravitational-wave burst detection problem *Phys. Rev.* D **95** 104046
[14] Cornish N J and Littenberg T B 2015 Bayeswave: Bayesian inference for gravitational wave bursts and instrument glitches *Class. Quantum Grav.* **32** 135012
[15] Abbott B P *et al* 2016 Characterization of transient noise in Advanced LIGO relevant to gravitational wave signal GW150914 *Class. Quantum Grav.* **33** 134001
[16] Nuttall L K *et al* 2015 Improving the data quality of advanced LIGO based on early engineering run results *Class. Quantum Grav.* **32** 245005
[17] et J A 2015 Characterization of the LIGO detectors during their sixth science run *Class. Quantum Grav.* **32** 115012
[18] McIver J 2012 Data quality studies of enhanced interferometric gravitational wave detectors *Class. Quantum Grav.* **29** 124010
[19] Allen B 2005 A chi-squared time-frequency discriminator for gravitational wave detection *Phys. Rev.* D **71** 062001
[20] Taracchini A *et al* 2014 Effective-one-body model for black-hole binaries with generic mass ratios and spins *Phys. Rev.* D **89** 061502
[21] Pürrer M 2016 Frequency domain reduced order model of aligned-spin effective-one-body waveforms with generic mass-ratios and spins *Phys. Rev.* D **93** 064041
[22] Abbott B P *et al* 2016 GW150914: first results from the search for binary black hole coalescence with advanced LIGO *Phys. Rev.* D **93** 122003
[23] Peters P C and Mathews J 1963 Gravitational radiation from point masses in a Keplerian orbit *Phys. Rev.* **131** 435–9
[24] Abbott B P *et al* 2016 Binary black hole mergers in the first advanced ligo observing run *Phys. Rev.* X **6** 041015
[25] Chatterji S *et al* 2004 Multiresolution techniques for the detection of gravitational-wave bursts *Class. Quantum Grav.* **21** S1809
[26] Nitz A 2017 Distinguishing short duration noise transients in LIGO data to improve the PyCBC search for gravitational waves from high mass binary black hole mergers (arXiv:1709.08974)
[27] Accadia T *et al* 2010 Noise from scattered light in virgo's second science run data *Class. Quantum Grav.* **27** 194011